

# Insights from *In Situ* Studies on the Early Stages of Platinum Nanoparticle Formation

Jette K. Mathiesen,<sup>#</sup> Jonathan Quinson,<sup>\*,#</sup> Alexandra Dworzak, Tom Vosch, Mikkel Juelsholt, Emil T. S. Kjær, Johanna Schröder, Jacob J. K. Kirkensgaard, Mehtap Oezaslan, Matthias Arenz,<sup>\*</sup> and Kirsten M. Ø. Jensen<sup>\*</sup>



Cite This: *J. Phys. Chem. Lett.* 2021, 12, 3224–3231



Read Online

ACCESS |



Metrics & More

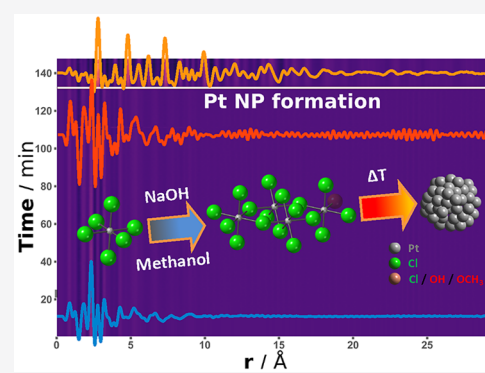


Article Recommendations



Supporting Information

**ABSTRACT:** Understanding the formation of nanomaterials down to the atomic level is key to rational design of advanced materials. Despite their widespread use and intensive study over the years, the detailed formation mechanism of platinum (Pt) nanoparticles remains challenging to explore and rationalize. Here, various *in situ* characterization techniques, and in particular X-ray total scattering with pair distribution function (PDF) analysis, are used to follow the structural and chemical changes taking place during a surfactant-free synthesis of Pt nanoparticles in alkaline methanol. Polynuclear structures form at the beginning of the synthesis, and Pt–Pt pair distances are identified before any nanoparticles are generated. The structural motifs best describing the species formed change with time, e.g., from [PtCl<sub>5</sub>–PtCl<sub>5</sub>] and [PtCl<sub>6</sub>–Pt<sub>2</sub>Cl<sub>6</sub>–PtCl<sub>6</sub>] to [Pt<sub>2</sub>Cl<sub>10</sub>–Pt<sub>3</sub>Cl<sub>8</sub>–Pt<sub>2</sub>Cl<sub>10</sub>]. The formation of these polynuclear structures with Pt–Pt coordination before the formation of the nanoparticles is suggested to account for the fast nucleation observed in the synthesis.



Precious metals such as Pt, Ir, Pd, Ag, or Au are essential materials for modern societies, for instance, due to their catalytic properties.<sup>1,2</sup> The increased demand on these limited resources call for new strategies to synthesize, process, and apply precious metal based materials more efficiently in the relevant technologies. An effective way to maximize the use of precious materials is to control their structure down to the atomic scale, which can be achieved by developing nanoparticles (NPs) with high surface-to-volume ratios.<sup>3</sup> Due to the strong structure–property relationships at the nanoscale, a detailed understanding of the mechanisms of nanomaterial synthesis is key to enable further breakthroughs in NP design. To rationally propose improved synthesis methods, the structural changes that take place when molecular precursors form precious metal nanomaterials must be better understood.

Platinum (Pt) is a material very broadly used for its many applications and a model system for nucleation theory of nanomaterials.<sup>4</sup> However, a detailed understanding of Pt NP formation is still lacking.<sup>4</sup> It is generally agreed that the formation of Pt NPs in wet-chemical syntheses proceeds via (i) a reduction step, followed by (ii) nucleation and (iii) particle growth.<sup>5</sup> The exact pathway (especially the nucleation step) appears to depend on experimental conditions,<sup>6</sup> the type of solvent and/or reducing agent,<sup>7</sup> the type of stabilizing agents,<sup>8</sup> and the precursor concentration.<sup>9</sup> Recently, some reports have suggested that Pt<sub>n</sub>Cl<sub>x</sub> species with several Pt–Pt bonds may play a role in the nucleation process,<sup>7</sup> whereas theoretical

studies have suggested a range of Pt<sub>n</sub>(0) clusters like Pt<sub>6</sub> or Pt<sub>9</sub> as key building blocks in the nucleation process.<sup>10,11</sup> Other studies point toward the formation of polynuclear Pt complexes stabilized by oxygen bridging groups<sup>12</sup> or chelating effects<sup>13</sup> before the formation of face-centered cubic (*fcc*) Pt NPs occurs. An overview of the different techniques that have previously been used to study Pt NP formation is given in the [Supporting Information](#).

To best follow the dynamic formation of Pt NPs at a molecular level and understand the structural changes that take place all the way from the initial precursor reduction over nucleation to particle growth, we use here various *in situ* characterization methods. In particular, X-ray total scattering with pair distribution function (PDF) analysis gives information on the distance between atoms in clusters, complexes, and molecules as well as nanomaterials with medium and long-range order.<sup>14–16</sup> The ability to retrieve structural information over a wide Ångstrom to nanometer range makes PDF especially well-suited to study the structural changes taking place upon formation of NPs in real time, all

Received: January 23, 2021

Accepted: March 22, 2021

Published: March 25, 2021



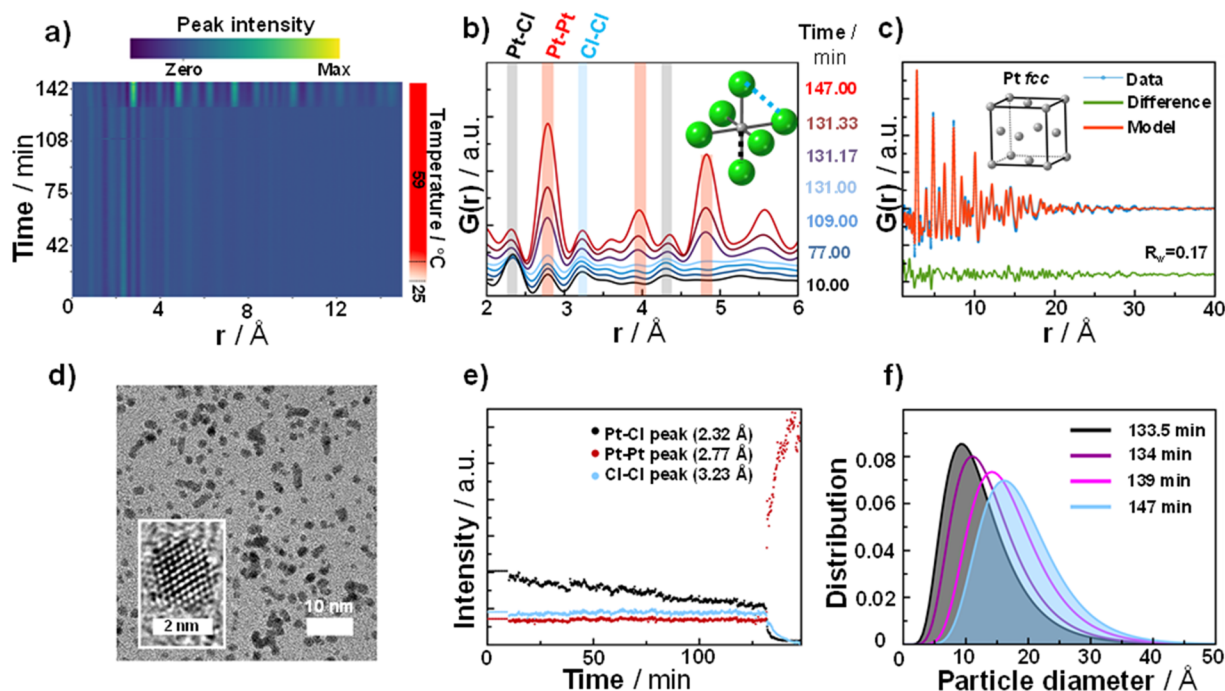


**Figure 1.** (a) *In situ* X-ray total scattering data of Pt NP formation showed as reduced Pair Distribution Function  $G(r)$  as a function of time. The color bar above the figure represents the PDF peak intensity, while the temperature scale is shown to the right of the figure. For the first 10 min of the experiment, the sample was kept at room temperature before heating to 59 °C. (b) Selected PDFs from different experiment times, where Pt–Cl, Cl–Cl, and Pt–Pt distances are indicated. The inset shows the octahedral  $\text{PtCl}_6$  structure present in the  $\text{H}_2\text{PtCl}_6$  precursor salt. (c) Real-space Rietveld refinement of PDF (blue) obtained 147 min into the experiment. The data were fitted with a Pt *fcc* model (red) in the  $r$ -range from 1.5 to 60 Å. The green curve displays the difference between model and data. The inset shows the Pt *fcc* model used for the refinement. (d) Example of TEM micrograph of Pt NPs obtained in alkaline methanol from  $\text{H}_2\text{PtCl}_6$ . Scale bar is 10 nm. Inset: high resolution TEM micrograph of a 2 nm Pt NP. The scale bar is 2 nm. (e) Evolution of selected PDF peak intensities as a function of synthesis time during the *in situ* experiments. The black, red, and blue data points correspond to the Pt–Cl, Pt–Pt, and Cl–Cl peak intensities, respectively. (f) Results from refinement of *in situ* X-ray total scattering data of Pt NP formation. Evolution of the size distribution after Pt NP nucleation. The size distribution observed 2.5 min after Pt NPs nucleate (black), during growth (purple and magenta), and at the end of the experiment (16 min after nucleation) are plotted.

the way from the precursor structure.<sup>17,18</sup> PDF has previously been used to study the formation of *fcc* Pt NPs in a fast (few minutes) synthesis under supercritical conditions<sup>14</sup> and is yet to be used to study more conventional synthesis conditions. In addition, and with rare exceptions, previous studies of colloidal Pt NP formation have always been performed in the presence of surfactants.<sup>7,13,19</sup> The role and/or the actual need for additives to stabilize Pt intermediates, like possible  $\text{Pt}_n\text{Cl}_x$  complexes, is therefore difficult to establish to date.<sup>20–22</sup> Here, we use a recently reported surfactant-free Pt NP synthesis, which is desirable for the development of nanoparticles for catalysis.<sup>23–27</sup> The surfactants used in many other NP syntheses block the active sites for heterogeneous and electrocatalysis, and time- and/or energy-consuming postsynthesis steps are therefore usually needed before as-synthesized Pt NPs can be applied. With the surfactant-free synthesis studied here, these challenges are avoided, as size-controlled Pt NPs are obtained in a low-boiling point solvent without the need for stabilizing agents. We here show that the surfactant-free synthesis is also ideal to study the formation mechanism of nanomaterials like Pt NPs.

**Formation and Growth of Pt NPs.** In the surfactant-free synthesis studied here, Pt NPs are formed from a solution of  $\text{H}_2\text{PtCl}_6$  and NaOH in methanol.<sup>28–33</sup> Upon heat treatment, the  $\text{H}_2\text{PtCl}_6$  precursor is converted to metallic NPs. We first use X-ray total scattering to follow the process. The *in situ* X-ray total scattering data obtained during the formation of *fcc* Pt NPs from  $\text{H}_2\text{PtCl}_6$  (50 mM) in alkaline (1 M NaOH)

methanol at 59 °C in 3 mm diameter glass tubes are given in Figure S1 in the form of the reduced structure function,  $F(Q)$ . Figure 1a,b show the corresponding PDFs, plotted as the reduced PDF denoted  $G(r)$ . Data from a repeat experiment are given in Figure S2. In the beginning of the experiment, PDF peaks are seen only in the range 1–10 Å, but after ca. 131 min of synthesis, the PDFs dramatically change and long-range order appears. At this point, all main PDF peaks can be assigned to the expected *fcc* Pt structure, and the experimental PDFs can be modeled using a bulk *fcc* Pt model, taking into account dampening due to NP size, as illustrated in Figure 1c. This sudden, burst-like formation of NPs is in agreement with previous observations,<sup>28,29,33</sup> and *in situ* SAXS studies of the synthesis reported in Figures S3 and S4. The PDF fit in Figure 1c allows extracting both information on the local structural arrangement and the average long-range structure, and the fit shows that the size of the Pt NPs at the end of the experiment (after 147 min) is around 2 nm; see Tables S1–S4. The small NP size with a narrow size distribution is in line with SAXS characterization in Figures S3 and S4 and TEM characterization in Figure 1d.

Figure 1e shows the intensity of PDF peaks assigned to Pt–Cl, Pt–Pt, and Cl–Cl pairs (discussed in detail below), plotted as a function of time. The intensity of the Pt–Cl peak (2.32 Å) decreases over time, while the Pt–Pt (2.77 Å) and Cl–Cl (3.23 Å) peak intensities are nearly constant until the Pt–Pt peak intensity at 2.77 Å suddenly increases as *fcc* Pt NPs nucleate. From the nucleation event at 131 min to the end of

the experiment after 147 min, the *fcc* Pt NPs grow from ca. 1 to 2 nm, illustrated in Figure 1f and Figures S5–S10.

**Effect of Alkaline Methanol on the Structures Formed in  $H_2PtCl_6$  Solutions.** We now qualitatively consider the PDF observed from the precursor solution, i.e., during the first 10 min of the experiment, where the reaction mixture was kept at room temperature. We first consider the PDF obtained from a  $H_2PtCl_6$  solution in the absence of a base, shown in Figure 2a,b. Here, only short-range order is present, marked by the

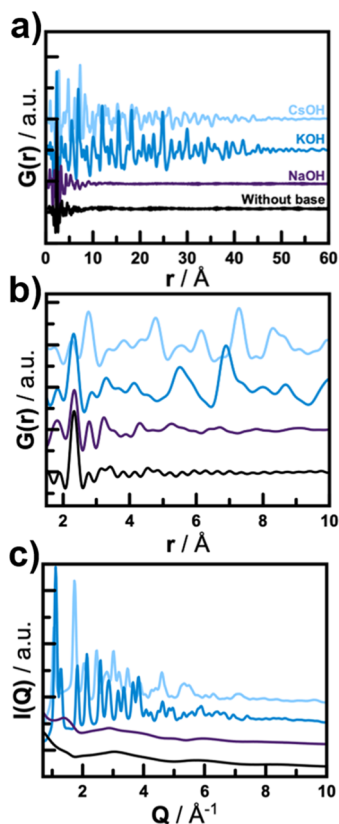


**Figure 2.** (a, b) PDFs and (c)  $I(Q)$  functions obtained in the presence and absence of base, showing the base-dependence in the formation of a longer-range structure. The data set obtained without base was also discussed by Quinson et al.<sup>31</sup> The scattering data from the samples prepared without base and with NaOH have been multiplied by 5.

absence of clear peaks above 5.0 Å. The structural motifs present in  $H_2PtCl_6$  solutions in methanol have previously been described as octahedral  $[PtCl_6]$ , square-planar  $[PtCl_4]$ , and  $[PtCl_x(OCH_3)_y]$  complexes with varying degree of methoxy substitution.<sup>6,14</sup> Our PDF also shows the presence of a small  $[PtCl_x]$  complex structure, and the most intense peak at ca. 2.30 Å can be assigned to Pt–Cl bond distances and the peak at ca. 3.20 Å to a Cl–Cl distance. The best fit of the PDF obtained from the precursor solution without the addition of base was obtained assuming an octahedral or square-planar  $[PtCl_x]$  structure with only one methoxy substituted; see Figure S11 and Table S5.<sup>31</sup> The square-planar structure is characteristic of complexes with Pt species in oxidation state II.<sup>14</sup> The presence of Pt(II) species in a freshly prepared solution of  $H_2PtCl_6$  is at first surprising but is consistent with XAS analysis, as described in Figures S12 and S13 and Table S6. The presence of Pt(II) species may be attributed to beam-induced or light-induced reduction.<sup>28,31,34,35</sup>

When a base (NaOH, KOH, or CsOH) is added to a  $H_2PtCl_6$  solution in methanol, PDF peaks from the precursor solution extend above 5 Å, as seen in Figure 2. Both the extent of structural order and the structure forming depends on the nature of the base used in the synthesis. A crystalline structure is found to instantly form upon addition of CsOH, which is observed in Figure 2c by the presence of intense Bragg peaks. The Bragg peaks arise from both *fcc* Pt NPs and crystalline  $Cs_2PtCl_6$ , and the PDF (Figure 2a) can be modeled with the two phases as illustrated in Figure S14. The fit shows ca. 83 wt %  $Cs_2PtCl_6$  and 17 wt % *fcc* Pt.  $Cs_2PtCl_6$  is insoluble in methanol and therefore precipitates by adding CsOH to the  $H_2PtCl_6$  precursor solution. In the case of KOH, we also observe the immediate formation of crystalline  $K_2PtCl_6$  (Figure S14), but no *fcc* Pt NPs are observed before heating.

With the smaller  $Na^+$  cation, no long-range order structure is formed; however, PDF peaks extend to ca. 7.0–8.0 Å.  $Na_2PtCl_6$  (and the stable hydrate  $Na_2PtCl_6 \cdot 6H_2O$ ) is soluble in methanol, and we therefore see no precipitation in the NaOH/ $H_2PtCl_6$  mixtures. Several sharp peaks can be identified in the PDF, which can be assigned to specific atomic pairs in  $[PtCl_6]$  in octahedral geometry<sup>14</sup> illustrated in Figure 1b, i.e., at ca. 2.30 Å (Pt–Cl) and 3.30 Å (Cl–Cl) as well as at higher  $r$ -values. The broad peak observed at 1.85 Å cannot be assigned to any known bond lengths in the octahedrally coordinated  $[PtCl_6]$  structure. Instead, the peak may arise from effects from background subtraction, and Fourier termination ripples. The medium range structure seen in the NaOH/ $H_2PtCl_6$  sample cannot be described by the known  $Na_2PtCl_6$  structure, although it does account for the presence of Pt–Cl and Cl–Cl peaks in the local PDF range. In Figure S15, the experimental PDF is also compared to that calculated from  $Na_2Pt(OH)_6$ , which could be expected to form. However, this structure also does not describe the experimental PDF data. These observations show that the precursor complexes forming in the  $H_2PtCl_6$ /NaOH methanol mixture mainly consist of  $[PtCl_x]$  units, rather than  $[Pt(OH)_x]$  units, but that their coordination in the medium order range is different from that seen in crystalline  $Na_2PtCl_6$  structure. Interestingly, a peak is also seen at ca. 2.80 Å, which corresponds well to Pt–Pt distances in metallic *fcc* Pt.<sup>7</sup> This first qualitative analysis of the precursor solution thus suggests the formation of a nanoscale polynuclear complex structure consisting of  $[PtCl_x]_n$  units, as well as Pt–Pt bonds. Possible  $Pt_nCl_x$  complexes are discussed further in the next section.

We have previously studied the role of NaOH, KOH, and CsOH on the stability of Pt NPs formed and the influence of the cations during synthesis.<sup>30</sup> The surfactant-free colloidal Pt NPs are stabilized in the decreasing order of the cation size  $Na^+ > K^+ \sim Cs^+$ . This can be attributed to the decreasing interaction of the cation with the negatively charged Pt particle surface. It was also observed that with NaOH, a clear yellow-orange solution of  $H_2PtCl_6$  in alkaline methanol is obtained leading to well-defined NPs after synthesis. In contrast, with KOH and CsOH a turbid solution is obtained leading to agglomerated NPs after synthesis.<sup>30</sup> This observation in light of the PDF data in Figure 2a suggests that the precursor structure and solubility affect the NP formation. These results certainly call for further investigations on the exact role of the cation on the nature of the long-range structure, but these considerations are beyond the scope of the present study.

**Precursor Complexes Formed in Alkaline NaOH Methanol.** We now turn to modeling of the precursor complexes formed in

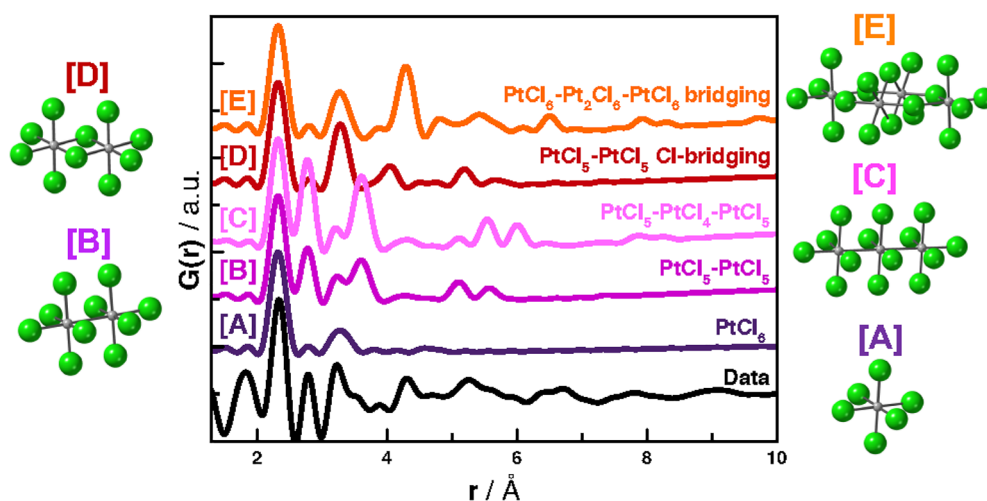


**Figure 3.** Structures and calculated PDFs of  $Pt_nCl_x$  complexes with various bonding environments. The calculated PDFs of structure [A] as a monomer  $[PtCl_6]$ , structure [B] as a dimer  $[PtCl_5-PtCl_5]$ , structure [C] as a linear trimer  $[PtCl_5-PtCl_4-PtCl_5]$ , structure [D] as a Cl-bridging dimer  $[PtCl_5-PtCl_5]$ , and structure [E] as a bridging dimer  $[PtCl_6-Pt_2Cl_6-PtCl_6]$ . The experimental data obtained from the precursor (black) in alkaline methanol (NaOH) are shown in the bottom of the figure.

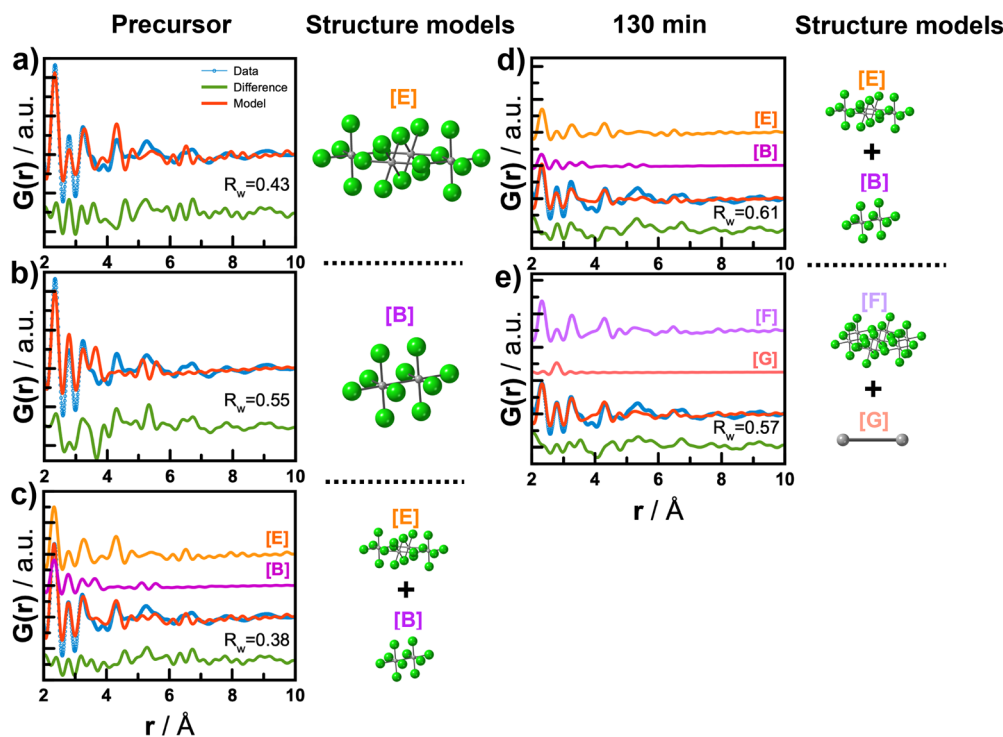


**Figure 4.** (a)–(c) Refinement of the PDF from the precursor solution. Single-phase refinement of the (a) bridging structure [E] and (b) linear dimer structure [B] to the experimental data. (c) Two-phase refinement of the experimental PDF data using the [E] and [B]. (Right) Representation of the structural models used in each refinement. (d) Refinement of the experimental data obtained just before Pt NP nucleation in the  $r$ -range of 2–10 Å. Two-phase PDF refinement using (d) structures [E] and [B] and (e) structures [F] and [G]. (Right) Representation of the structural models used in each refinement.

the  $H_2PtCl_6/NaOH$  methanol solution. As described above, it is clear from the local range of the PDF that the structure is mainly built up from  $[PtCl_x]$  units. This is confirmed when modeling the PDFs using the structural motifs previously proposed in precursor solutions, such as  $[PtCl_6]$ ,<sup>14</sup>  $[PtCl_4]$ ,<sup>14</sup>  $[PtCl_5(OCH_3)]$ ,<sup>6</sup> and  $[PtCl_3OCH_3]$ <sup>6</sup> (Figures S16–S18 and Table S7). Here, the Pt–Cl and Cl–Cl peaks are well described, but the observed features above 3.0 Å are not included in any of the models. Most importantly, the use of NaOH in the synthesis gives rise to a Pt–Pt peak at ca. 2.8 Å.

To account for this, we considered simple linear polynuclear  $Pt_nCl_x$  structures previously suggested.<sup>7</sup> Following this structural suggestion, several structural models of mono-, di-, and trimeric complexes were considered and the PDFs of each model calculated. Each calculated model was compared to the experimental PDF, which is presented in Figure 3. Most previously suggested models with either linear Pt–Pt bonding (structure [B] and [C] in Figure 3) or Cl-bridging (structure [D] in Figure 3) fail to describe the observed peak at 4.3 Å; see Figures S19–23 and a further discussion in the Supporting

**Information.** Another way of connecting two  $[\text{PtCl}_6]$  units is through bridging  $\text{PtCl}_x$  units, which has previously been seen in  $\text{Au}_n\text{Cl}_x$  and  $\text{Pt}_n\text{Cl}_x$  complexes.<sup>36,37</sup> As illustrated with structure [E] in Figure 3, the bridging can occur through two  $[\text{PtCl}_6]$  units, which are connected through Cl-bridging. Further representation of this  $[\text{PtCl}_6-\text{Pt}_2\text{Cl}_6-\text{PtCl}_6]$  motif can be found in Figure S24A. This motif provides both Pt–Cl and Cl–Cl pair correlations to the model and more importantly it introduces an additional PDF peak at ca. 4.3 Å, corresponding to the distance between a Pt atom in the  $[\text{PtCl}_6]$  motif and a Pt atom in the bridge. However, the relative intensities of the PDF peaks present do not agree with the experimental PDF.

Figure 3 shows that no single polynuclear structure was found to account for all the features observed in the experimental PDF. However, by combining two models, each describing features seen in the experimental PDF, the PDF from the precursor complex structure in NaOH and methanol before heating up can be represented: structure [B], a linear dimer composed of  $[\text{PtCl}_5-\text{PtCl}_5]$  units connected by Pt–Pt bonds and structure [E], a bridging dimer,  $[\text{PtCl}_6-\text{Pt}_2\text{Cl}_6-\text{PtCl}_6]$ . The calculated PDFs of the two suggested structures account relatively well for the features above 3 Å. Furthermore, a combined model is also in agreement with the local structure ( $r < 5$  Å). Fits using each of the structures, as well as a two-phase fit are shown in Figure 4a–c. The two-phase fit provides a better agreement factor in comparison to the single-phase refinements. The parameters resulting from the presented refinements are reported in Table S8.

It is crucial to note that the two structures proposed should not be seen as uniquely present in the precursor solution. Our analysis rather shows that the sample does not contain monodisperse ionic clusters, as we have previously been able to identify in other *in situ* PDF studies of NP formation, where better agreement factors can be obtained.<sup>38</sup> Here, the model represents the dominating structural motifs that are present in the sample, and the precursor complexes are not expected to be composed of separate linear and bridging dimer units. Instead, the data indicate that the precursor consist of a polymeric type structure, containing both linear Pt–Pt bonds and Cl–Cl bonds connecting  $\text{PtCl}_x$  monomers. A trimer structure did not describe the PDF well, which is presented as structure [C] in Figure 3. However, this does not rule out the presence of a longer Pt–Pt–Pt chain, since PDF peaks corresponding to atomic pairs in nonrigid structures over large lengths scale may be smeared out and hard to identify.<sup>39</sup> Note also that cluster–solvent correlations, or coordination to  $\text{Na}^+$  ions, remain a general challenge to date for modeling. The effects are not taken into account in the modeling here, which may also affect the fit quality.

**Temporal Evolution of Polynuclear Complexes.** Figure 1e shows the intensity of the peaks assigned to Pt–Cl, Pt–Pt, and Cl–Cl pairs in the PDF, plotted as a function of time. The evolution of the Pt–Cl peak intensity is in line with XAS analysis reported in Figures S25 and S26 and Table S9. The structural changes are also reflected when the structure models applied above are fitted to the PDF obtained just before *fcc* Pt NP formation (1 min before formation, i.e., 130 min into the experiment). This fit is illustrated in Figure 4d, and the  $R_w$  value (a fit agreement factor) increases from 0.36 for the precursor PDF to 0.61 for the PDF obtained just prior to Pt NP formation (130 min of synthesis).

Figure 1e shows that while the Pt–Cl intensity decreases, the Pt–Pt peak intensity only slightly increases. On the basis of

the structural models proposed for the precursor complexes above, we can suggest scenarios agreeing with the observations. First, a reduction of the linear  $\text{PtCl}_x$  complexes can be described by including a hypothetical, linear  $\text{Pt}_2$  structure, [G], in the PDF refinement. This will decrease the ratio between Pt–Cl and Pt–Pt distances and therefore provide the behavior as displayed in Figure 1e. As seen in Figure S27, the introduction of the linear, hypothetical  $\text{Pt}_2$  model in the two-phase PDF refinement provides a slightly better description of the Pt–Pt and Pt–Cl peak intensities. The introduction of a  $\text{Pt}_2$  structure does not propose isolated  $\text{Pt}_2$  units being formed. Instead, it suggests that more Pt–Pt bonding might occasionally occur within the polynuclear complexes. Considering the models [B] and [E] proposed for the initial polynuclear precursor complex structures in Figure 4a, a second way of reducing the Pt–Cl peak intensity, while keeping Cl–Cl interactions, is to consider the bridging dimer presented at structure [E]. The average Pt–Cl coordination in the structure can be reduced from 4.5 to 4 by extending the structure through condensation of two  $[\text{PtCl}_6-\text{Pt}_2\text{Cl}_6-\text{PtCl}_6]$  units.

Combining the extended structure, denoted structure [F], with the  $\text{Pt}_2$  structure [G] did provide a slightly better description of the experimentally observed PDF, as shown in Figure 4e. The parameters resulting from refinements can be found in Table S10, while a further representation of structure [F] is given in Figure S24B. Other polynuclear complex structures, such as  $[\text{Pt}_2\text{Cl}_8-\text{Pt}_3\text{Cl}_8-\text{Pt}_2\text{Cl}_8]$  (Figure S28 and Table S11), were also considered, although this did not improve the fit. Here, however, it is crucial again to note that the models proposed should not be seen as unique representations of the structure present right before nucleation, but rather containing the structural motifs that are involved in the reaction.

The time-resolved EXAFS data indicate an increase in Pt–Pt coordination during the first stages of the reaction, increasing from ca. 1 to 3; see Figure S25 and Table S9. This is in line with the increasing number of Pt in the polynuclear Pt complexes and the need to introduce the hypothetical  $\text{Pt}_2$  motif for PDF fitting as discussed above. Alternatively, the hypothetical  $\text{Pt}_2$  motif could also be a possible building block within larger  $\text{Pt}_n$  clusters. Various DFT calculations have suggested the planar triangular  $\text{Pt}_6$  configuration to be a stable cluster structure and key building block to larger  $\text{Pt}_n$  clusters.<sup>10,11</sup> Although the  $\text{Pt}_6$  configuration has been suggested by DFT calculations, it is not possible with the current experimental PDF or EXAFS data to validate the presence of  $\text{Pt}_n$  structures, probably due to the very short lifetime of this putative intermediate. In summary, the analysis of the time-resolved PDF and EXAFS data show that the Pt–Cl coordination decreases during the induction period of the reaction. The structures present before Pt NP nucleation are thus likely to be a combination of  $\text{Pt}_n\text{Cl}_x$  complexes and structures with various sizes/lengths, different degrees of Cl substitution and valence state of Pt species. In addition, XAS, Raman, and UV–vis data detailed and discussed in the Supporting Information point toward a likely hydroxyl/methoxy substitution of some of the here identified  $\text{Pt}_n\text{Cl}_x$  complexes, Figure S29–S34.

In conclusion, using *in situ* PDF analysis, *in situ* XAS, *in situ* Raman spectroscopy, *in situ* SAXS, and a surfactant-free synthesis of colloidal *fcc* Pt NPs, it is shown that structures containing Pt–Pt bonding are formed in alkaline methanol before *fcc* Pt NP nucleation. It is therefore established that no

surfactants are needed to stabilize polynuclear  $Pt_nCl_x$  complex structures, which seems to play a role in the nucleation and formation of Pt NPs.

A pathway for *fcc* Pt NP formation from  $H_2PtCl_6$  in alkaline methanol is proposed in Figure 5. Rapidly after addition of

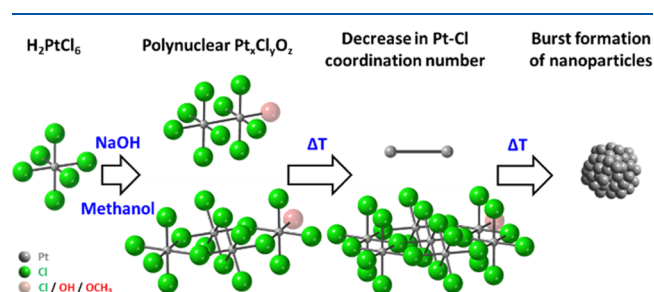


**Figure 5.** Schematic representation of the reaction pathway from  $H_2PtCl_6$  to Pt NPs in alkaline methanol.

NaOH, polynuclear  $Pt_nCl_x$  complexes are formed. These are not monodisperse, magic-sized structures, since no discrete value of  $x$  can be evaluated. During heating, the Pt–Cl coordination number decreases, while the Pt–Pt coordination number increases. Upon a burst-like formation event,<sup>40</sup> *fcc* Pt NPs are found to form, which grows over time as more NPs are found to nucleate. While this general behavior is compatible with the formation of Pt NPs generally believed to follow a four-step mechanism involving double autocatalysis,<sup>41</sup> we here give molecular and structural insights into this phenomenon. Our results suggest that the burst formation is likely related to the formation of complex Pt structures with preformed Pt–Pt bonds.

These findings are relevant to develop further syntheses of precious metal NPs and nanomaterials, in particular by surfactant-free approaches, which are well-suited for readily active catalysts.<sup>29</sup> The results call for further study to understand not only the possible role of precursor concentration and the role of cations as evidenced in this work but also the role of solvent or the effect of additives in the nature of the species formed and their influence on the nucleation and formation of NPs. Driven by the observations presented here, studies on the generality of  $M_nCl_x$  intermediates in the formation of other NPs is under investigation, where M is a metal atom from different precursors. As our knowledge increases on nanomaterial formation, it is likely that no single model can explain all nucleation and growth processes. Nevertheless, the insight gained here using *in situ* PDF completed with other *in situ* characterization techniques pave the way to detailed investigation of the formation of colloidal NPs to develop more complex and performing nanomaterials by controlled wet-chemical syntheses.

## ■ ASSOCIATED CONTENT

### SI Supporting Information

The Supporting Information is available free of charge at <https://pubs.acs.org/doi/10.1021/acs.jpcllett.1c00241>.

Experimental section, background characterization, repeated experiments, X-ray scattering data, PDF, SAXS, XAS, Raman and UV–vis data (PDF)

## ■ AUTHOR INFORMATION

### Corresponding Authors

**Jonathan Quinson** – Department of Chemistry, University of Copenhagen, 2100 Copenhagen Ø, Denmark; [orcid.org/0000-0002-9374-9330](https://orcid.org/0000-0002-9374-9330); Email: [jonathan.quinson@chem.ku.dk](mailto:jonathan.quinson@chem.ku.dk)

**Matthias Arenz** – Department of Chemistry and Biochemistry, University of Bern, CH-3012 Bern, Switzerland; [orcid.org/0000-0001-9765-4315](https://orcid.org/0000-0001-9765-4315); Email: [matthias.arenz@dcb.unibe.ch](mailto:matthias.arenz@dcb.unibe.ch)

**Kirsten M. Ø. Jensen** – Department of Chemistry, University of Copenhagen, 2100 Copenhagen Ø, Denmark; [orcid.org/0000-0003-0291-217X](https://orcid.org/0000-0003-0291-217X); Email: [kirsten@chem.ku.dk](mailto:kirsten@chem.ku.dk)

### Authors

**Jette K. Mathiesen** – Department of Chemistry, University of Copenhagen, 2100 Copenhagen Ø, Denmark

**Alexandra Dworzak** – School of Mathematics and Science, Department of Chemistry, Carl von Ossietzky University of Oldenburg, 26111 Oldenburg, Germany; Technical Electrocatalysis Laboratory, Institute of Technical Chemistry, Technical University of Braunschweig, 38106 Braunschweig, Germany

**Tom Vosch** – Department of Chemistry, University of Copenhagen, 2100 Copenhagen Ø, Denmark; [orcid.org/0000-0001-5435-2181](https://orcid.org/0000-0001-5435-2181)

**Mikkel Juulsholt** – Department of Chemistry, University of Copenhagen, 2100 Copenhagen Ø, Denmark; [orcid.org/0000-0001-6401-8267](https://orcid.org/0000-0001-6401-8267)

**Emil T. S. Kjær** – Department of Chemistry, University of Copenhagen, 2100 Copenhagen Ø, Denmark

**Johanna Schröder** – Department of Chemistry and Biochemistry, University of Bern, CH-3012 Bern, Switzerland; [orcid.org/0000-0001-5461-4751](https://orcid.org/0000-0001-5461-4751)

**Jacob J. K. Kirkensgaard** – Department of Food Science, University of Copenhagen, 1958 Frederiksberg C, Denmark; [orcid.org/0000-0001-6265-0314](https://orcid.org/0000-0001-6265-0314)

**Mehtap Oezaslan** – School of Mathematics and Science, Department of Chemistry, Carl von Ossietzky University of Oldenburg, 26111 Oldenburg, Germany; Technical Electrocatalysis Laboratory, Institute of Technical Chemistry, Technical University of Braunschweig, 38106 Braunschweig, Germany; [orcid.org/0000-0001-8545-7576](https://orcid.org/0000-0001-8545-7576)

Complete contact information is available at: <https://pubs.acs.org/doi/10.1021/acs.jpcllett.1c00241>

### Author Contributions

#J.K.M. and J.Q. contributed equally.

### Notes

The authors declare no competing financial interest.

## ■ ACKNOWLEDGMENTS

K.M.Ø.J., J.Q., J.K.M., and M.J. are grateful to the Villum Foundation for financial support though a Villum Young Investigator grant (VKR00015416). K.M.Ø.J. acknowledges the Carlsberg Foundation for financial support through grant CF14-0652 and CF17-0976. This research used resources of the Advanced Photon Source, a U.S. Department of Energy (DOE) Office of Science User Facility operated for the DOE Office of Science by Argonne National Laboratory under Contract No. DE-AC02-06CH11357. The authors are grateful

to the staff of beamline 11-ID-B at Argonne National Laboratory for support during the PDF experiments. The Danish Research Council is acknowledged for covering travel expenses in relation to the synchrotron experiment (DanScatt). The Swiss Light Source (SLS), Switzerland is thanked for beamtime access to the SuperXAS beamline (proposal ID 20190183). A.D. and M.O. acknowledge the Deutsche Forschungsgemeinschaft (DFG) under contract number of OE610/1-1 within the research unit FOR2213 ([www.nagocat.de](http://www.nagocat.de)). Drs. L. Theil Kuhn and S. B. Simonsen, Technical University of Denmark, are thanked for access to TEM facilities and their help in HRTEM acquisition. Profs B. W. Laursen and T. J. Sorensen, University of Copenhagen are thanked for use of UV-vis equipment. SuperXAS beamline scientists and in particular Drs. M. Nachttegaal and A. Clark are thanked. Mr. V. Mints and Dr. F. Bizzotto are thanked for their help in the XAS data acquisition.

## REFERENCES

- (1) Seh, Z. W.; Kibsgaard, J.; Dickens, C. F.; Chorkendorff, I. B.; Norskov, J. K.; Jaramillo, T. F. Combining theory and experiment in electrocatalysis: Insights into materials design. *Science* **2017**, *355* (6321), eaad4998.
- (2) Xu, G.; Yano, J.; Sakai, S.-I. Recycling potentials of precious metals from end-of-life vehicle parts by selective dismantling. *Environ. Sci. Technol.* **2019**, *53* (2), 733–742.
- (3) Losch, P.; Huang, W. X.; Goodman, E. D.; Wrasman, C. J.; Holm, A.; Riscoe, A. R.; Schwalbe, J. A.; Cargnello, M. Colloidal nanocrystals for heterogeneous catalysis. *Nano Today* **2019**, *24*, 15–47.
- (4) Quinson, J.; Jensen, K. M. Ø. From platinum atoms in molecules to colloidal nanoparticles: a review on reduction, nucleation and growth mechanisms. *Adv. Colloid Interface Sci.* **2020**, *286*, 102300.
- (5) Thanh, N. T. K.; Maclean, N.; Mahiddine, S. Mechanisms of nucleation and growth of nanoparticles in solution. *Chem. Rev.* **2014**, *114* (15), 7610–7630.
- (6) Chen, S. M.; Yang, Q. Y.; Wang, H. H.; Zhang, S.; Li, J.; Wang, Y.; Chu, W. S.; Ye, Q.; Song, L. Initial reaction mechanism of platinum nanoparticle in methanol-water system and the anomalous catalytic effect of water. *Nano Lett.* **2015**, *15* (9), 5961–5968.
- (7) Yao, T.; Liu, S. J.; Sun, Z. H.; Li, Y. Y.; He, S.; Cheng, H.; Xie, Y.; Liu, Q. H.; Jiang, Y.; Wu, Z. Y.; Pan, Z. Y.; Yan, W. S.; Wei, S. Q. Probing nucleation pathways for morphological manipulation of platinum nanocrystals. *J. Am. Chem. Soc.* **2012**, *134* (22), 9410–9416.
- (8) Leong, G. J.; Schulze, M. C.; Strand, M. B.; Maloney, D.; Frisco, S. L.; Dinh, H. N.; Pivovar, B.; Richards, R. M. Shape-directed platinum nanoparticle synthesis: nanoscale design of novel catalysts. *Appl. Organomet. Chem.* **2014**, *28* (1), 1–17.
- (9) Cheong, S.; Watt, J.; Ingham, B.; Toney, M. F.; Tilley, R. D. In Situ and ex situ studies of platinum nanocrystals: Growth and evolution in solution. *J. Am. Chem. Soc.* **2009**, *131* (40), 14590–14595.
- (10) Chaves, A. S.; Rondina, G. G.; Piotrowski, M. J.; Tereshchuk, P.; Da Silva, J. L. F. The role of charge states in the atomic structure of  $\text{Cu}_n$  and  $\text{Pt}_n$  ( $n = 2–14$  atoms) clusters: A DFT investigation. *J. Phys. Chem. A* **2014**, *118* (45), 10813–10821.
- (11) Kumar, V.; Kawazoe, Y. Evolution of atomic and electronic structure of Pt clusters: Planar, layered, pyramidal, cage, cubic, and octahedral growth. *Phys. Rev. B: Condens. Matter Mater. Phys.* **2008**, *77* (20), 205418.
- (12) Borodko, Y.; Ercius, P.; Zherebetskyy, D.; Wang, Y.; Sun, Y.; Somorjai, G. From single atoms to nanocrystals: photoreduction of  $\text{PtCl}_6^{2-}$  in aqueous and tetrahydrofuran solutions of PVP. *J. Phys. Chem. C* **2013**, *117* (50), 26667–26674.
- (13) Borodko, Y.; Ercius, P.; Pushkarev, V.; Thompson, C.; Somorjai, G. From single Pt atoms to Pt nanocrystals: Photoreduction of  $\text{Pt}^{2+}$  inside of a PAMAM dendrimer. *J. Phys. Chem. Lett.* **2012**, *3* (2), 236–241.
- (14) Saha, D.; Bojesen, E. D.; Jensen, K. M. O.; Dippel, A. C.; Iversen, B. B. Formation mechanisms of Pt and  $\text{Pt}_3\text{Gd}$  nanoparticles under solvothermal conditions: An in situ total X-ray scattering study. *J. Phys. Chem. C* **2015**, *119* (23), 13357–13362.
- (15) Chupas, P. J.; Chapman, K. W.; Jennings, G.; Lee, P. L.; Grey, C. P. Watching nanoparticles grow: The mechanism and kinetics for the formation of  $\text{TiO}_2$ -supported platinum nanoparticles. *J. Am. Chem. Soc.* **2007**, *129* (45), 13822–13824.
- (16) Quinson, J.; Inaba, M.; Neumann, S.; Swane, A. A.; Bucher, J.; Simonsen, S. B.; Kuhn, L. T.; Kirkensgaard, J. J. K.; Jensen, K. M. O.; Oezaslan, M.; Kunz, S.; Arenz, M. Investigating particle size effects in Catalysis by Applying a Size-Controlled and Surfactant-Free Synthesis of Colloidal Nanoparticles in alkaline ethylene glycol: Case study of the oxygen reduction reaction on Pt. *ACS Catal.* **2018**, *8* (7), 6627–6635.
- (17) Bojesen, E. D.; Iversen, B. B. The chemistry of nucleation. *CrystEngComm* **2016**, *18* (43), 8332–8353.
- (18) Jensen, K. M. Ø.; Tyrsted, C.; Bremholm, M.; Iversen, B. B. In situ studies of solvothermal synthesis of energy materials. *ChemSusChem* **2014**, *7* (6), 1594–1611.
- (19) Yao, T.; Sun, Z. H.; Li, Y. Y.; Pan, Z. Y.; Wei, H.; Xie, Y.; Nomura, M.; Niwa, Y.; Yan, W. S.; Wu, Z. Y.; Jiang, Y.; Liu, Q. H.; Wei, S. Q. Insights into initial kinetic nucleation of gold nanocrystals. *J. Am. Chem. Soc.* **2010**, *132* (22), 7696–7701.
- (20) Heuer-Jungemann, A.; Feliu, N.; Bakaimi, I.; Hamaly, M.; Alkilany, A.; Chakraborty, I.; Masood, A.; Casula, M. F.; Kostopoulou, A.; Oh, E.; Susumu, K.; Stewart, M. H.; Medintz, I. L.; Stratakis, E.; Parak, W. J.; Kanaras, A. G. The role of ligands in the chemical synthesis and applications of inorganic nanoparticles. *Chem. Rev.* **2019**, *119* (8), 4819–4880.
- (21) Reichenberger, S.; Marzun, G.; Muhler, M.; Barcikowski, S. Perspective of surfactant-free colloidal nanoparticles in heterogeneous catalysis. *ChemCatChem* **2019**, *11* (18), 4489–4518.
- (22) Koczur, K. M.; Mourdikoudis, S.; Polavarapu, L.; Skrabalak, S. E. Polyvinylpyrrolidone (PVP) in nanoparticle synthesis. *Dalton Trans.* **2015**, *44* (41), 17883–17905.
- (23) Cargnello, M.; Chen, C.; Diroll, B. T.; Doan-Nguyen, V. V. T.; Gorte, R. J.; Murray, C. B. Efficient removal of organic ligands from supported nanocrystals by fast thermal annealing enables catalytic studies on well-defined active phases. *J. Am. Chem. Soc.* **2015**, *137* (21), 6906–6911.
- (24) Naresh, N.; Wasim, F. G. S.; Ladewig, B. P.; Neergat, M. Removal of surfactant and capping agent from Pd nanocubes (Pd-NCs) using tert-butylamine: its effect on electrochemical characteristics. *J. Mater. Chem. A* **2013**, *1* (30), 8553–8559.
- (25) Park, J. Y.; Aliaga, C.; Renzas, J. R.; Lee, H.; Somorjai, G. A. The role of organic capping layers of platinum nanoparticles in catalytic activity of CO oxidation. *Catal. Lett.* **2009**, *129* (1–2), 1–6.
- (26) Huang, W. X.; Hua, Q.; Cao, T. Influence and removal of capping ligands on catalytic colloidal nanoparticles. *Catal. Lett.* **2014**, *144* (8), 1355–1369.
- (27) Li, D. G.; Wang, C.; Tripkovic, D.; Sun, S. H.; Markovic, N. M.; Stamenkovic, V. R. Surfactant removal for colloidal nanoparticles from solution synthesis: The effect on catalytic performance. *ACS Catal.* **2012**, *2* (7), 1358–1362.
- (28) Quinson, J.; Kacenauskaitė, L.; Bucher, J.; Simonsen, S. B.; Kuhn, L. T.; Oezaslan, M.; Kunz, S.; Arenz, M. Controlled synthesis of surfactant-free water-dispersible colloidal platinum nanoparticles by the Co4Cat process. *ChemSusChem* **2019**, *12* (6), 1229–1239.
- (29) Quinson, J.; Neumann, S.; Wannmacher, T.; Kacenauskaitė, L.; Inaba, M.; Bucher, J.; Bizzotto, F.; Simonsen, S. B.; Kuhn, L. T.; Bujak, D.; Zana, A.; Arenz, M.; Kunz, S. Colloids for catalysts: A concept for the preparation of superior catalysts of industrial relevance. *Angew. Chem., Int. Ed.* **2018**, *57* (38), 12338–12341.
- (30) Quinson, J.; Bucher, J.; Simonsen, S. B.; Theil Kuhn, L.; Kunz, S.; Arenz, M. Monovalent alkali cations: simple and eco-friendly

stabilizers for surfactant-free precious metal nanoparticle colloids. *ACS Sustainable Chem. Eng.* **2019**, *7* (16), 13680–13686.

(31) Quinson, J.; Mathiesen, J. K.; Schroder, J.; Dworzak, A.; Bizzotto, F.; Zana, A.; Simonsen, S. B.; Theil Kuhn, L.; Oezaslan, M.; Jensen, K. M. Ø.; Arenz, M. Teaching old precursors new tricks: fast room temperature synthesis of surfactant-free colloidal platinum nanoparticles. *J. Colloid Interface Sci.* **2020**, *577*, 319–328.

(32) Quinson, J.; Kacenauskaite, L.; Schoder, J.; Simonsen, S. B.; Theil Kuhn, L.; Vosch, T.; Arenz, M. UV-induced syntheses of surfactant-free precious metal nanoparticles in alkaline methanol and ethanol. *Nanoscale Adv.* **2020**, *2*, 2288–2292.

(33) Quinson, J.; Neumann, S.; Kacenauskaite, L.; Bucher, J.; Kirkensgaard, J. J. K.; Simonsen, S. B.; Theil Kuhn, L.; Zana, A.; Vosch, T.; Oezaslan, M.; Kunz, S.; Arenz, M. Solvent-dependent growth and stabilization mechanisms of surfactant-free colloidal Pt nanoparticles. *Chem. - Eur. J.* **2020**, *26* (41), 9012–9023.

(34) Kacenauskaite, L.; Swane, A. A.; Kirkensgaard, J. J. K.; Fleige, M.; Kunz, S.; Vosch, T.; Arenz, M. Synthesis mechanism and influence of light on unprotected platinum nanoparticles synthesis at room temperature. *ChemNanoMat* **2016**, *2* (2), 104–107.

(35) Kacenauskaite, L.; Quinson, J.; Schultz, H.; Kirkensgaard, J. J. K.; Kunz, S.; Vosch, T.; Arenz, M. UV-Induced synthesis and stabilization of surfactant-free colloidal Pt nanoparticles with controlled particle size in ethylene glycol. *ChemNanoMat* **2017**, *3* (2), 89–93.

(36) Casas, J. M.; Diosdado, B. E.; Fornies, J.; Garcia-Monforte, M. A.; Laporta, R.; Martin, A.; Tomas, M. Synthesis and characterization of binuclear Pt(IV) complexes and tetranuclear mixed valence complexes of Platinum(II)-Platinum(IV). *J. Organomet. Chem.* **2019**, *897*, 130–138.

(37) Dell'Amico, D. B.; Calderazzo, F.; Marchetti, F.; Merlino, S.; Perego, G. X-Ray crystal and molecular structure of Au<sub>4</sub>Cl<sub>8</sub>, the product of the reduction of Au<sub>2</sub>Cl<sub>6</sub> by Au(CO)Cl. *J. Chem. Soc., Chem. Commun.* **1977**, *1*, 31–32.

(38) Juelsholt, M.; Lindahl Christiansen, T.; Jensen, K. M. Ø. Mechanisms for tungsten oxide nanoparticle formation in solvothermal synthesis: From polyoxometalates to crystalline materials. *J. Phys. Chem. C* **2019**, *123* (8), 5110–5119.

(39) Tyrsted, C.; Lock, N.; Jensen, K. M. O.; Christensen, M.; Bojesen, E. D.; Emerich, H.; Vaughan, G.; Billinge, S. J. L.; Iversen, B. B. Evolution of atomic structure during nanoparticle formation. *IUCr* **2014**, *1* (3), 165–171.

(40) Whitehead, C. B.; Watzky, M. A.; Finke, R. G. "Burst nucleation" vs autocatalytic, "burst" growth in near-monodisperse particle-formation reactions. *J. Phys. Chem. C* **2020**, *124* (45), 24543–24554.

(41) Besson, C.; Finney, E. E.; Finke, R. G. Nanocluster nucleation, growth, and then agglomeration kinetic and mechanistic studies: A more general, four-step mechanism involving double autocatalysis. *Chem. Mater.* **2005**, *17* (20), 4925–4938.